

Article

# Magnetic Emissions from Brake Wear are the Major Source of Airborne Particulate Matter Bioaccumulated by Lichens Exposed in Milan (Italy)

Aldo Winkler<sup>1,\*</sup> , Tania Contardo<sup>2</sup>, Andrea Vannini<sup>2</sup>, Sergio Sorbo<sup>3</sup>, Adriana Basile<sup>4</sup> and Stefano Loppi<sup>2,\*</sup> 

<sup>1</sup> Istituto Nazionale di Geofisica e Vulcanologia, 00143 Rome, Italy

<sup>2</sup> Department of Life Sciences, University of Siena, 53100 Siena, Italy; tania.contardo2@unisi.it (T.C.); andrea.vannini@unisi.it (A.V.)

<sup>3</sup> Centro Servizi Metrologici e Tecnologici Avanzati, University of Naples Federico II, 80138 Napoli, Italy; sersorbo@unina.it

<sup>4</sup> Department of Biology, University of Naples Federico II, 80138 Napoli, Italy; adriana.basile@unina.it

\* Correspondence: aldo.winkler@ingv.it (A.W.); stefano.loppi@unisi.it (S.L.);  
Tel.: +39-(0)6-5186-0325 (A.W.); +39-(0)577-233-740 (S.L.)

Received: 21 February 2020; Accepted: 11 March 2020; Published: 19 March 2020



**Abstract:** The concentration of selected trace elements and the magnetic properties of samples of the lichen *Evernia prunastri* exposed for 3 months in Milan (Italy) were investigated to test if magnetic properties can be used as a proxy for the bioaccumulation of chemical elements in airborne particulate matter. Magnetic analysis showed intense properties driven by magnetite-like minerals, leading to significant correlations between magnetic susceptibility and the concentration of Fe, Cr, Cu, and Sb. Selected magnetic particles were characterized by Scanning Electron Microscope and Energy Dispersion System microanalyses, and their composition, morphology and grain size supported their anthropogenic, non-exhaust origin. The overall combination of chemical, morphoscopic and magnetic analyses strongly suggested that brake abrasion from vehicles is the main source of the airborne particles accumulated by lichens. It is concluded that magnetic susceptibility is an excellent parameter for a simple, rapid and cost-effective characterization of atmospheric trace metal pollution using lichens.

**Keywords:** magnetic biomonitoring; particulate matter; lichen transplants; brake wear; urban air pollution

## 1. Introduction

It has been estimated that more than 4 million people die annually for health problems caused by poor air quality [1]. Air quality in urban areas is a great concern worldwide, since most of the human population lives in cities that quite often do not meet the air quality standards, thus being exposed to high levels of pollutants [2]. Particulate matter (PM) is by far the most important air pollutant in urban areas [3], and short- and long-term exposure to PM is responsible for a wide array of negative effects on human health, spanning from inflammations, cardio-vascular diseases, and lung cancer [1]. Therefore, monitoring air pollution in urban areas is crucial for human health.

Automated stations are often used for monitoring air quality over time and space, but a real high-resolution network is often lacking owing to the constraints of establishing and maintaining sophisticated and costly equipment. Thus, biological monitoring (biomonitoring) may turn very useful in supporting and complementing the limited data derived from instrumental monitoring. In addition, biomonitoring may in turn help to improve the knowledge on the response of organisms to pollutants.

Among living organisms, lichens are well-known very sensitive bioindicators of air pollution, which can act as real biological sentinels [4]. Unlike higher plants, lacking roots, stomata and waxy cuticles, lichens are completely dependent on atmospheric wet and dry deposition for nutrients, and there is evidence that their elemental content do reflect bulk atmospheric deposition [5]. Lichens are especially useful in urban areas, where the complexity of the environment and the great variety of pollution sources make monitoring quite a difficult task [6]. In addition, lichen biomonitoring can be used in cases of environmental forensics and environmental justice [7,8]. The use of lichen transplants, i.e., samples taken from a background area and exposed into the study area, has recently overcome the use of native samples due to the possibility of planning any sampling design, controlling exactly the exposure time, and comparing the results with pre-exposure values [9].

Urban PM may have remarkable magnetic properties related to the content of anthropogenic iron oxides, mostly magnetite-like ferrimagnetic particles. Magnetic nanoparticles (NPs), formed by combustion and/or friction-derived, which are common in urban airborne PM, were recently found even in the human brain, where they can enter directly through the olfactory nerve [10]. Exposure to up to ~22 billion magnetic NPs/g of ventricular tissue appears to be directly associated with early and significant cardiac damage in children and young adults [11].

Heavy metals are often associated to the magnetic fraction of PM, arising directly from the emission sources (e.g., brakes), or incorporated in the iron oxides' structure during combustion processes (fuel exhausts, industrial emissions). Therefore, the magnetic properties of PM often constitute original, cheap and fast proxies of the anthropogenic fraction of PM, with immediate health-related interest.

Among biological media, plant leaves and lichens turned out to be extremely suitable for magnetic biomonitoring of air pollution in urban areas (for a review see [12]), shedding light on the bioaccumulation of anthropogenic dust and providing location-specific and time-integrated air quality information.

In this study, a biomonitoring survey of air quality using lichen transplants was carried out in Milan (Italy), investigating the trace element content and the magnetic properties of exposed samples. A Bayesian statistical approach was used to test if magnetic properties can be used as a proxy for the bioaccumulation of chemical elements.

## 2. Materials and Methods

### 2.1. Study Area

The city of Milan, with 1.4 million inhabitants, is one of the most densely populated city in Italy. The city is located in the Po plain, a region notoriously characterized by thermal inversion, stagnation of air masses, continental-like climate type (mean annual temperature and rainfall are 13.1 °C and 1013 mm, respectively), with long and severe winters and high temperatures (up to 38 °C) in summer. These unfavorable characteristics make this area one of the most polluted by PM of Italy as well as of Europe, with the main pollution sources being vehicular traffic, heating systems, railway lines, and the nearby airport.

### 2.2. Lichen Sampling

The epiphytic (tree-inhabiting) lichen species *Evernia prunastri* (L.) Ach was selected for this study, being widely used in similar biomonitoring studies [13–15] and in spite of its documented capacity to bioaccumulate great amounts of trace elements and to reflect atmospheric deposition [5]. In addition, the fruticose (shrubby) growth form of this lichen allows easy handling of thalli. Apparently healthy thalli were collected from deciduous oak trees in a forested remote area of Tuscany (Central Italy), far removed from roads and any local pollution sources. Thalli were left to acclimate for 24 h in a climatic chamber at 16 °C, 40  $\mu\text{mol m}^{-2} \text{s}^{-1}$  photons PAR (photoperiod of 12 h) and RH = 65% before preparation of samples. After cleaning with plastic tweezers from extraneous material such as bark or

insects, samples of ca. 2 g were arranged into lichen bags made of plastic net (Figure 1) that were kept in a climatic chamber at 16 °C, 40  $\mu\text{mol m}^{-2} \text{s}^{-1}$  photons PAR (photoperiod of 12 h) and RH = 65% until transplant. Samples were transplanted within 1 week from collection. Before transplantation, sample vitality was randomly evaluated by analyzing the photosynthetic efficiency, which resulted in being optimal.



**Figure 1.** A lichen bag exposed in the study area.

Samples were transplanted at 25 sites in Milan, selected following a stratified random design according to distance from the center (three belts: central, semiperipheral, peripheral), and the nine administrative city districts. In addition, a control site was selected at a relatively unpolluted forested area 50 km N of Milan, far from roads and local pollution sources. At each exposure site (and at the control site), five lichen bags were exposed from December 2018 to February 2019 at a height of ca. 2 m from ground, tied to the branches of lime (*Tilia* sp.) trees located along roads or inside parks. The exposure period (winter) was selected in such a way to assure a high metabolic activity of samples [8,15]; the duration of exposure of 3 months is regarded as optimal for *E. prunastri* [9]. After the exposure, samples were retrieved, air-dried and stored in paper bags at  $-20$  °C until analysis. For the analysis, the lichen material inside each lichen bag was pooled. Having a control site accounting also for the possible effect of transplantation, unexposed samples were not assayed.

### 2.3. Chemical Analysis

The concentration of selected elements (Al, As, Cd, Cr, Cu, Fe, Pb, Sb, Zn) was assessed by ICP-MS (Sciex Elan 6100, Perkin-Elmer, Waltham, MA, USA) after wet acid mineralization (3 mL 70%  $\text{HNO}_3$ , 0.2 mL of 60% HF and 0.5 mL  $\text{H}_2\text{O}_2$ ) in a microwave digestion system (Ethos 900, Milestone, Bomby Municipality, Denmark). A procedural blank and a sample of the certified reference material IAEA-336 “lichen” were included in each batch of samples. Recoveries were in the range of 90%–113% and the precision of analysis, expressed as relative standard deviation of five replicates, was within 10% for all elements. Results are expressed on a dry weight basis.

#### 2.4. Magnetic Analysis

Dry lichen samples were placed in standard 8 cm<sup>3</sup> palaeomagnetic plastic cubes for the analysis of magnetic susceptibility and in pharmaceutical gel caps #4 for the hysteresis measurements. Mass magnetic susceptibility ( $k$ ) was calculated dividing the values measured with a KLY5 Agico meter for the net weight of the samples. The coercive force ( $B_c$ ), the saturation remanent magnetization by mass ( $M_{rs}$ ) and the saturation magnetization by mass ( $M_s$ ) were measured using a vibrating sample magnetometer (Micromag 3900, PMC) equipped with a carbon fibre probe, under cycling in a maximum field of 1.0 T. Concentration dependent hysteresis parameters were calculated subtracting the high field paramagnetic linear trend before dividing the magnetic moments for the net weight of the samples. The coercivity of remanence ( $B_{cr}$ ) values were extrapolated from backfield remagnetization curves up to  $-1$  T, following forward isothermal remanent magnetization up to a  $+1$  T field.

The percentage decay of  $M_{rs}$  after 100 s was calculated as:

$$M_{rs} (SP)\% = 100 \times (M_{rs0} - M_{rs100})/M_{rs0}, \quad (1)$$

where SP refers to the superparamagnetic fraction,  $M_{rs0}$  is the remanent magnetization measured as soon as the magnetic field is reduced to noise levels after the application of a 1 T field, and  $M_{rs100}$  is the remanence measured 100 s later. The values of  $M_{rs} (SP)\%$  are indicative of the fraction of remanent magnetization due to viscous magnetic components, which are usually carried by ultrafine magnetic particles, dimensionally in the superparamagnetic/stable single domain boundary, which is around 20–35 nm for magnetite [16,17].

The domain state and magnetic grain-size of the samples were compared to theoretical magnetite according to the hysteresis ratios  $M_{rs}/M_s$  vs.  $B_{cr}/B_c$  in the “Day plot” [18–20].

First order reversal curves (FORCs) [21,22] were measured using the Micromag operating software; FORC diagrams were processed, smoothed and drawn with the FORCINEL Igor Pro routine [23]. FORCs were measured in steps of 2.5 mT, with 300 ms averaging time and maximum applied field being 1.0 T. The optimum smoothing factor was evaluated by FORCINEL software.

#### 2.5. Morphoscopic Observations

Fragments from representative thalli were cut into pieces, mounted onto carbon stubs and then coated with carbon in an Automatic Carbon Coater (Agar Scientific, Essex, UK). The sample surfaces were observed under a Scanning Electron Microscopy (SEM Jeol JSM-5310) equipped with an INCA Energy Dispersive Spectroscopy (EDS) system. Micrographs and spectra were collected with a 15 KV operating voltage, 50–70  $\mu$ A current, 20 mm work distance, and a 15–17 spot size (JSM-5310 data). Micrographs were acquired by an INCA image capture system; spectra were collected by an INCA X-stream pulse processor.

#### 2.6. Statistical Analysis

The magnitude of the relationship (effect size) between magnetic parameters and each bioaccumulated element was evaluated by the coefficient of determination  $R^2$ , which estimates the proportion of variance shared by the two variables, as explained by a linear model. As recommended for environmental data [24], the probability of the effect size was estimated using the highest posterior density intervals following a Bayesian approach [25]. In addition, Cohen’s  $f^2$  was also calculated [26] to class the effect size into small, medium and large [27]. Only  $R^2$  values at the lower point of the 95% credible interval scored at least as medium size effect according to Cohen’s  $f^2$  were retained. Prior to analysis, data were transformed to logarithms to achieve normal distributions, and centered to zero means in such a way that the intercept represents the value of the response variable at the mid-point of the predictor range, and the original variance is retained. All calculations were done with the free software R [28].

### 3. Results

#### 3.1. Bioaccumulation of Trace Elements

Lichen thalli transplanted at the control site showed values (Table 1) well within the range of background concentrations for this species [29]. After 3 months of exposure in Milan, samples of *E. prunastri* exhibited accumulation for all elements at all sites, with very few exceptions (Table 1), with mean values exceeding those of the control sample by a factor 1.2 (Cd) to 6.3 (Sb). Differences in concentrations across sites were in some cases remarkable, e.g., for Cu, which ranged between 6.5 and 55.4  $\mu\text{g/g dw}$ .

**Table 1.** Concentrations ( $\mu\text{g/g dw}$ ) of trace elements in samples of the lichen *Evernia prunastri* exposed for 3 months at 25 sites in Milan, as well as at a control site (ctrl).

Sample	Al	As	Cd	Cr	Cu	Fe	Pb	Sb	Zn
1	422	0.28	0.072	3.7	11.4	841	4.4	0.49	42.8
2	723	0.35	0.065	5.4	28.6	1269	5.6	0.95	36.8
3	504	0.34	0.065	3.8	18.2	777	6.3	0.73	32.7
4	279	0.25	0.059	2.3	6.5	471	4.1	0.55	33.8
5	599	0.26	0.064	3.4	18.4	696	3.8	0.60	31.8
6	428	0.31	0.074	6.9	55.4	932	5.8	0.83	36.8
7	521	0.31	0.083	3.7	17.0	850	5.4	0.89	52.0
8	882	0.37	0.066	4.2	14.6	959	4.4	0.72	32.6
9	656	0.37	0.073	3.9	29.1	923	6.0	0.79	60.5
10	509	0.28	0.070	2.9	8.9	631	4.1	0.51	27.1
11	927	0.39	0.069	5.3	37.2	1253	4.6	1.38	46.7
12	700	0.33	0.081	3.1	12.0	737	8.4	0.57	32.4
13	657	0.31	0.080	3.0	11.2	720	3.4	0.41	17.1
14	941	0.29	0.055	3.9	11.8	895	4.4	0.58	28.1
15	639	0.32	0.077	3.3	13.8	790	5.1	0.77	34.0
16	537	0.40	0.077	4.0	17.0	814	4.9	0.89	40.3
17	1066	0.34	0.070	4.2	20.2	1061	6.6	0.96	44.4
18	517	0.27	0.096	2.7	8.0	678	5.3	0.51	43.7
19	449	0.30	0.058	2.8	6.6	666	3.9	0.56	28.3
20	524	0.29	0.065	4.1	22.8	912	6.5	0.91	39.5
21	459	0.30	0.065	3.2	17.8	740	8.2	0.81	50.0
22	563	0.29	0.103	2.8	9.8	640	11.3	0.59	25.0
23	569	0.32	0.077	4.2	24.4	901	8.3	0.83	42.1
24	718	0.35	0.094	3.9	15.2	871	17.5	1.10	53.9
25	616	0.30	0.088	3.0	16.0	719	16.4	1.01	37.2
ctrl	429	0.21	0.061	1.7	3.3	442	2.0	0.12	27.1

#### 3.2. Magnetic Measurements

Magnetic susceptibility of *E. prunastri* transplants (Table 2) ranged between 7.8 and  $35.8 \times 10^{-8} \text{ m}^3 \text{ kg}^{-1}$ , always exceeding 6–29 times the value of the control sample ( $1.2 \times 10^{-8} \text{ m}^3 \text{ kg}^{-1}$ ) (Figure 2).

**Table 2.** Magnetic parameters of samples of the lichen *Evernia prunastri* exposed for 3 months at 25 sites in Milan, as well as at a control site (ctrl). k = mass magnetic susceptibility ( $10^{-8} \text{ m}^3\text{kg}^{-1}$ ), Ms = mass saturation magnetization ( $\text{mAm}^2\text{kg}^{-1}$ ), Mrs = mass saturation remanent magnetization ( $\text{mAm}^2\text{kg}^{-1}$ ), Bc = coercivity (mT), Bcr = coercivity of remanence (mT), SIRM/k = saturation isothermal remanent magnetization by magnetic susceptibility ratio (kA/m).

Sample	k	Ms	Mrs	Bc	Bcr	Bcr/Bc	Mrs/Ms	SIRM/k
1	13.31	9.06	0.52	5.84	37.20	6.37	0.06	3.93
2	26.10	25.16	1.66	7.06	40.88	5.79	0.07	6.35
3	12.49	8.51	0.53	6.01	38.74	6.44	0.06	4.23
4	8.77	7.32	0.45	5.53	35.83	6.48	0.06	5.19
5	16.38	19.41	0.94	4.88	40.71	8.35	0.05	5.72
6	20.32	20.57	1.45	6.89	40.75	5.92	0.07	7.14
7	13.72	10.04	0.63	5.59	40.33	7.21	0.06	4.63
8	17.07	20.68	1.16	5.41	39.09	7.23	0.06	6.82
9	13.21	9.07	0.56	5.86	37.55	6.41	0.06	4.24
10	8.78	7.58	0.53	6.18	38.45	6.23	0.07	6.07
11	35.85	32.66	1.53	4.41	33.89	7.68	0.05	4.27
12	9.70	6.39	0.35	5.72	37.53	6.55	0.05	3.62
13	8.73	6.48	0.48	6.51	34.63	5.32	0.07	5.46
14	14.63	7.31	0.44	6.15	35.72	5.81	0.06	3.01
15	14.62	16.25	0.83	4.62	39.82	8.62	0.05	5.65
16	11.98	12.54	0.70	5.27	38.95	7.39	0.06	5.83
17	22.93	15.81	0.82	4.86	37.23	7.67	0.05	3.57
18	10.02	10.52	0.65	5.44	32.76	6.02	0.06	6.53
19	10.71	8.33	0.40	4.67	34.69	7.42	0.05	3.74
20	26.02	23.71	1.36	5.38	37.73	7.01	0.06	5.22
21	17.17	8.44	0.42	5.03	35.08	6.97	0.05	2.43
22	7.75	5.95	0.39	6.22	36.69	5.90	0.07	4.99
23	27.11	20.97	1.14	5.50	38.65	7.03	0.05	4.21
24	15.53	13.22	0.94	6.26	37.36	5.96	0.07	6.03
25	9.22	9.31	0.55	5.26	37.88	7.20	0.06	5.96
ctrl	1.23	1.36	0.09	3.80	23.09	6.08	0.07	7.21

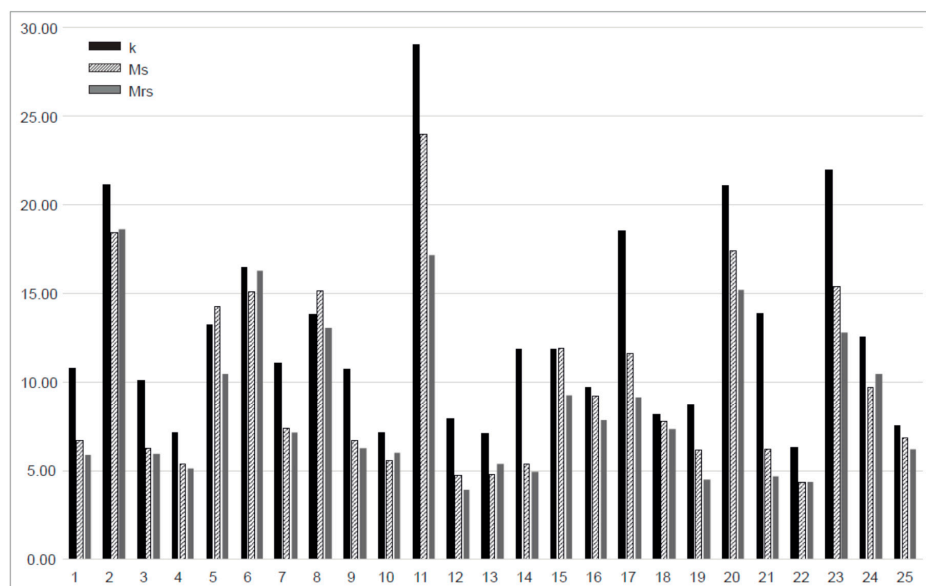


**Figure 2.** Histograms of the concentration-dependent magnetic parameters, normalized to the control sample; black columns for magnetic susceptibility (k), dithered for Ms, grey for Mrs.

All the hysteresis loops (Figure 3a,d) were similar in shape, narrow, saturated well before 1T, with a modest variability of both coercivities [ $4.4 \text{ mT} < B_c < 7.1 \text{ mT}$ ;  $32.8 \text{ mT} < B_{cr} < 40.9 \text{ mT}$ ]

(Table 2). The concentration-dependent magnetic parameters (Table 2) varied less than one order of magnitude [ $6.0 < M_s \text{ (mAm}^2\text{kg}^{-1}) < 32.7$ ;  $0.4 < M_{rs} \text{ (mAm}^2\text{kg}^{-1}) < 1.7$ ] and, similarly to susceptibility measurements, were 4–24 and 4–19 times in excess of the values of the control sample ( $M_s = 1.4 \text{ mAm}^2\text{kg}^{-1}$ ;  $M_{rs} = 0.1 \text{ mAm}^2\text{kg}^{-1}$ ) (Figure 2).

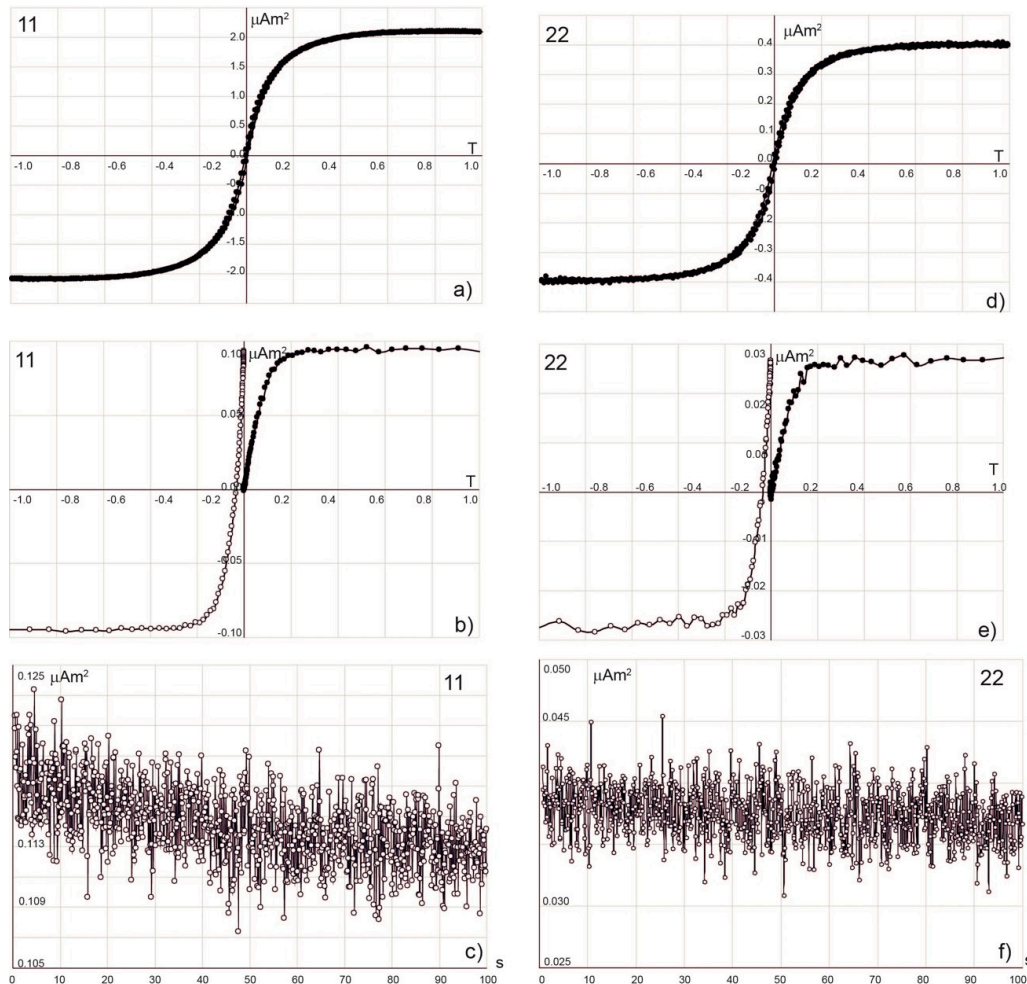


**Figure 3.** Hysteresis loops corrected for high-field linear trend (a,d), isothermal remanent magnetization and backfield application (b,e) and  $M_{rs}$  decay in 100 s (c,f) for samples 11 and 22, the most and the least intense of the dataset, respectively. Original data, not divided by mass.

Overall, the hysteresis parameters indicated slightly variable concentrations of very similar soft ferrimagnetic minerals, presumably ascribable to magnetite. Consistently with susceptibility measurements,  $M_s$  and  $M_{rs}$  values were always higher than in the control sample. It was not possible to estimate the Curie temperature by means of magnetothermic curves, given the low susceptibility values and the noisy behaviour caused by burning of organic matter during heating.

$M_{rs}$  (SP)% was estimated for samples 11 and 22 (Figure 3e,f), the most and the least intense of the dataset, respectively, and showed that the contribution of rapidly decaying components to the overall magnetization is about 5%–6%. This result is only indicative, as errors are large due to the relatively low values of magnetization and the short averaging time (100 ms).

The  $M_{rs}/M_s$  vs.  $B_{cr}/B_c$  ratios (Figure 4) indicated that the samples were distributed in the middle-right side of the plot, between the theoretical curves calculated for mixtures of single domain (SD) and multidomain (MD) magnetite grains and that calculated for a mixture of SD and superparamagnetic (SP) magnetite grains [19,20].

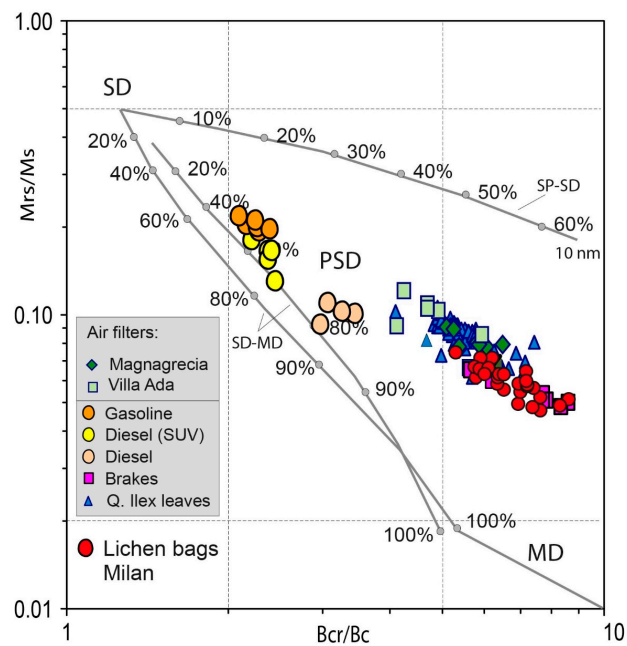


**Figure 4.** Bilogarithmic Day plot of the hysteresis ratios  $M_{rs}/M_s$  vs.  $B_{cr}/B_c$  for transplanted lichens *Evernia prunastri* (red dots) compared with *Quercus ilex* leaves from high traffic areas of Rome (green triangles) [30], air filters from monitoring stations in Rome (green diamonds and squares) [31], different kinds of fuel exhausts (orange, yellow and pink dots) and brake dusts (purple squares) [32]. The SD (single domain), PSD (pseudo-single domain) and MD (multidomain) fields and the theoretical mixing trends for SD-MD and SP-SD pure magnetite particles (SP, superparamagnetic) are taken from Dunlop [19,20]. Modified after [32].

FORC diagrams (Figure 5) were made for two samples (11 and 20), selected for their relatively intense magnetic properties; the distribution peaked close to the origin of the diagram and was dominated by viscous components of magnetization, typical for MD grains, without the asymmetrical features which usually suggest the presence of SP ultrafine particles. The two FORC diagrams are substantially identical, confirming that the samples contain variable concentrations of alike magnetic particles.

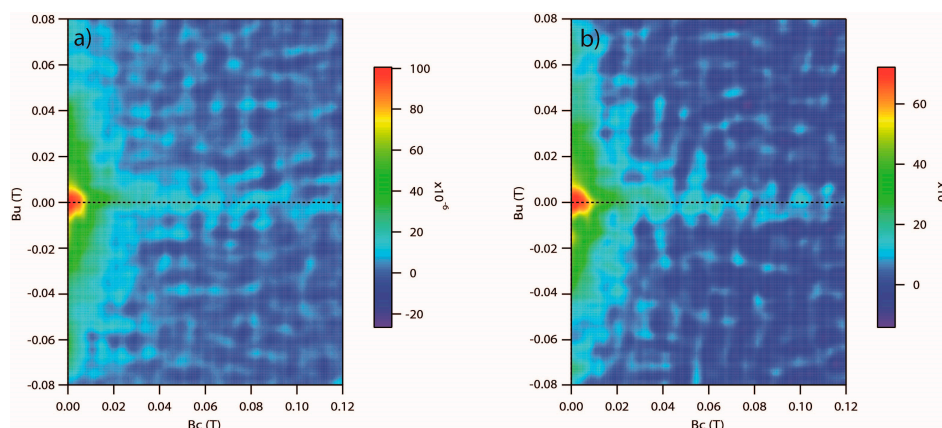


**Figure 5.** FORC (First Order Reversal Curve) diagrams for samples 11 (a) and 20 (b); the smoothing factor was 5 and 4, respectively.

### 3.3. Morphoscopic Observations

Morphoscopic observations (Figure 6) clearly showed the accumulation of Fe-rich particles, ranging from clusters of submicrometric grains (Figure 6a) to  $>10 \mu\text{m}$ , as well as coarser and sometimes flaky

metallic residuals (Figure 6b). Their chemical composition, as determined by EDS X-ray microanalysis, in addition to Fe, highlighted the widespread presence of elements such as Zn, Cu and Ba (Figure 6c). The shape and the recurrent inclusion of various elements other than Fe make these magnetic particles different from natural stoichiometric magnetite. Most morphologies were irregular, with rough and/or rounded and frictional surfaces, dissimilar to the spherical shapes of industrial fly ashes originated by the combustion of black and brown coal (e.g., [33–36]) or waste electrical and electronic equipment [37].

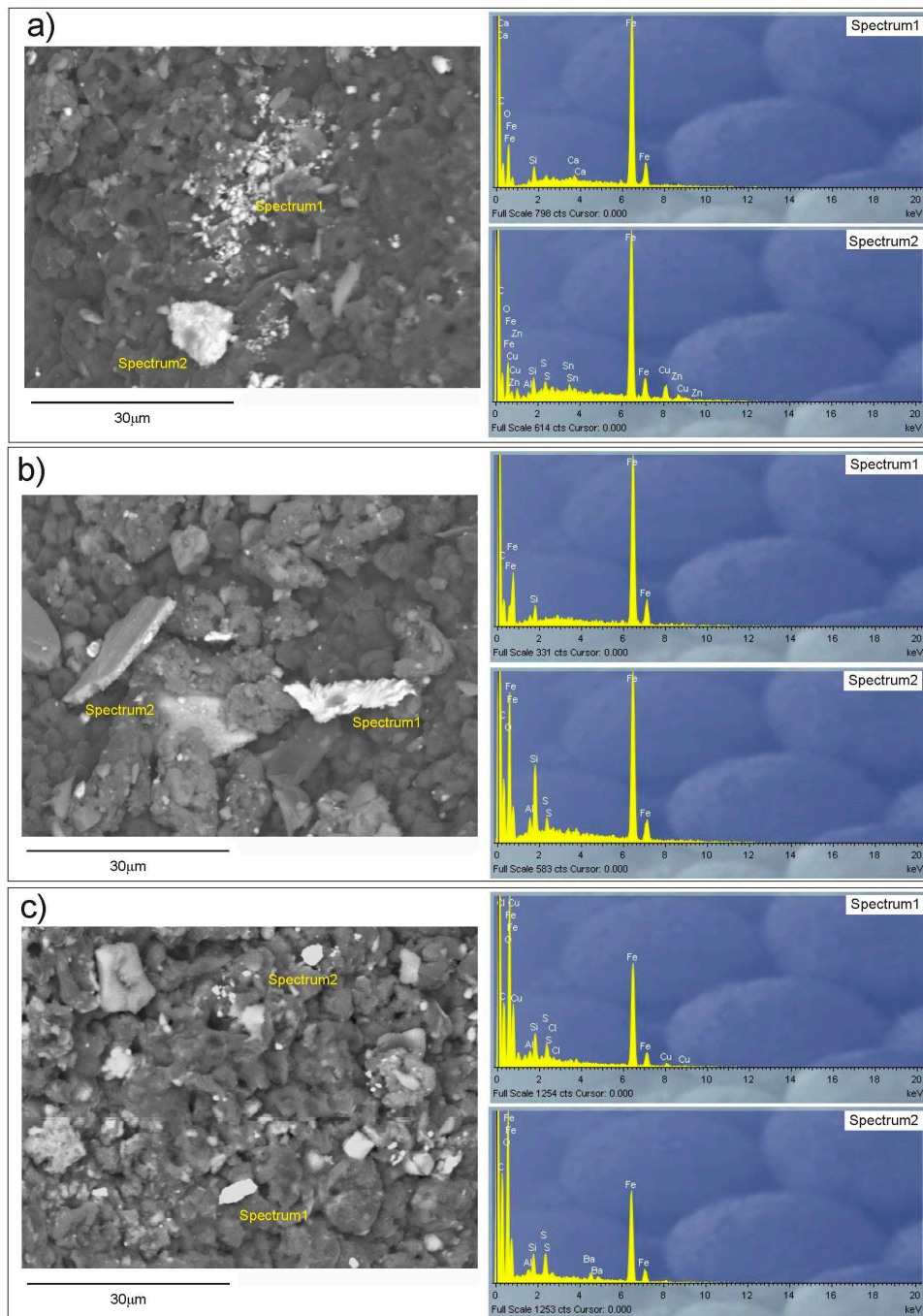


**Figure 6.** FESEM images and EDS spectra of selected particles embedded in the lichens exposed in Milan; (a) Spectrum 1; cluster of submicrometric Fe-rich particles; (b) coarse and flaky iron-rich residuals; (c) micrometric particles, rich in Fe, Cu and Ba.

### 3.4. Effect Size

Figure 7 shows the relationships between magnetic susceptibility and element concentrations, along with the 95% credible intervals (95CIs) of the  $R^2$  values. The latter, along with the respective Cohen's  $f^2$  output, are detailed in Table 3.

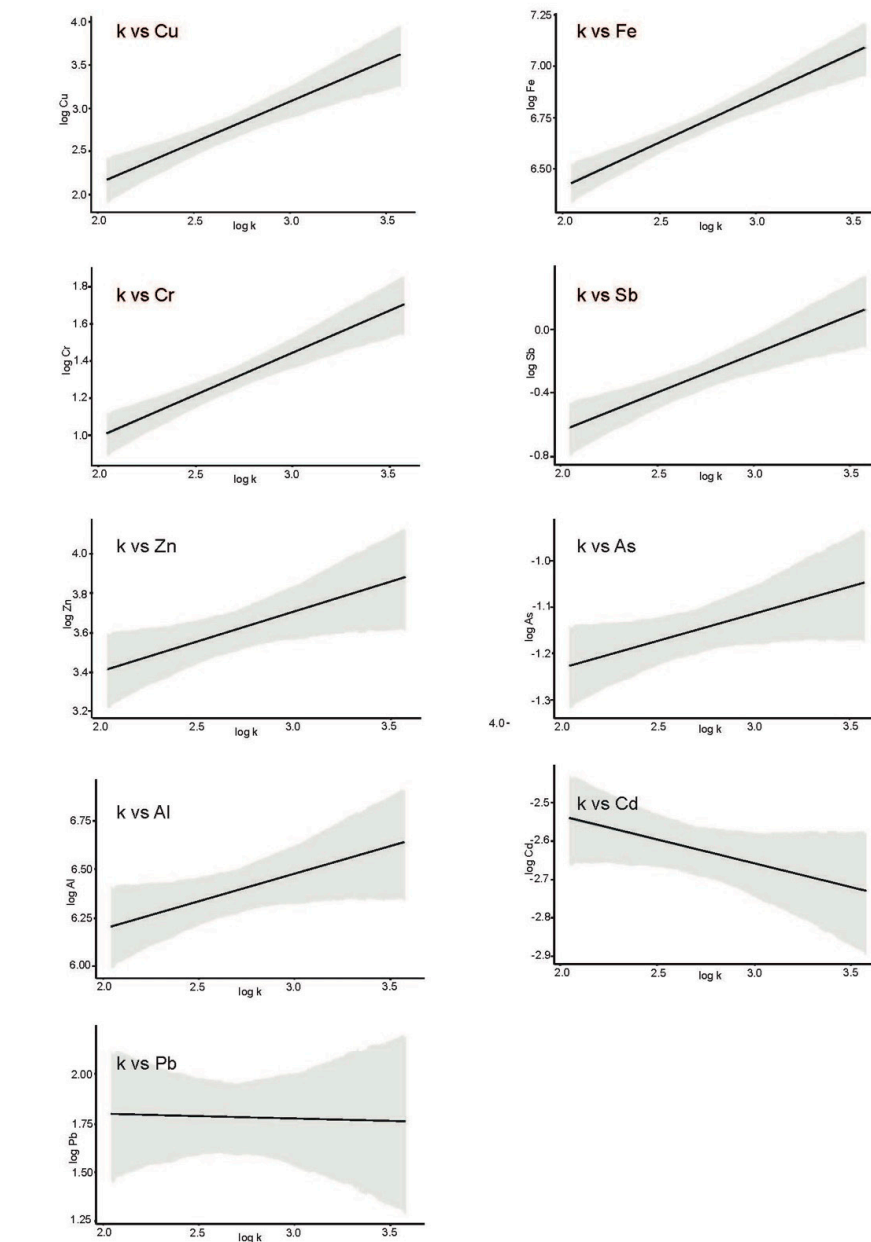


**Figure 7.** Relationships between magnetic susceptibility and element concentrations, along with the 95% credible intervals of the regression line.

Only the correlations with Fe, Cr, Cu, and Sb showed a Cohen's  $f^2$  at least medium. In addition, 95CIs of the  $R^2$  values as well as Cohen's  $f^2$  were calculated also between the four chemical elements above (data not shown), showing strong intercorrelations among all elements, with Cohen's  $f^2$  always > medium. Aluminium, which is a major element in the Earth's crust and has limited metabolic significance in lichens, is commonly used as a tracer of geogenic inputs, and correlations with this element are roughly taken as an indication of soil contamination of samples [38]. 95CIs of  $R^2$  and Cohen's  $f^2$  of Al with Fe, Cr, Cu and Sb (data not shown) highlighted only the correlation Al–Fe

( $R^2 = 0.20\text{--}0.63$ ,  $f^2 = 0.25$  “medium”). Magnetic susceptibility was also very well correlated with the other two concentration-dependent magnetic parameters Ms and Mrs (Table 3).

**Table 3.** Ninety-five percent credible intervals of the  $R^2$  values, Cohen’s  $f^2$  and magnitude of the effect size between magnetic susceptibility and chemical elements as well as other magnetic parameters.

	$R^2$	Cohen’s $f^2$	Effect Size
Al	0.00–0.36	0.00	small
As	0.00–0.36	0.00	small
Cd	0.00–0.30	0.00	small
Cr	0.43–0.73	0.75	large
Cu	0.36–0.70	0.56	large
Fe	0.51–0.76	1.04	large
Pb	0.00–0.14	0.00	small
Sb	0.23–0.64	0.30	medium
Zn	0.00–0.41	0.00	small
Ms	0.66–0.82	1.94	large
Mrs	0.51–0.76	1.04	large

#### 4. Discussion

The results of bioaccumulation showed that Milan is quite homogeneously affected by high deposition loads of elements such as Cr, Cu, Fe, and Sb; some more spotted peaks emerged also for Pb. This outcome is consistent with other lichen biomonitoring studies in urban areas of Italy [37,39–42]. The results are indicative of a common origin of pollutants from non-exhaust sources of vehicular traffic, such as brake abrasion. As a matter of fact, the above elements are used as components of brake systems [43], and brake abrasion is reported as the main source of trace elements in PM [44].

This conclusion is supported by the results of EDS X-ray microanalysis, which pinpointed the massive presence of Fe, and the widespread occurrence of Zn, Cu and Ba, the latter usually being connected with emissions from car brakes and tyres [32,45]. In addition, as shown by SEM analysis, Fe-rich particles are generally different from industrial spherical combustion particles, further indicating that their source are motor vehicles and more specifically, relying on their composition, brake abrasion [32].

The range of the magnetic susceptibility values ( $7.8$  to  $35.8 \times 10^{-8} \text{ m}^3\text{kg}^{-1}$ ), when compared with previous studies on transplanted lichens, is indicative of a notable concentration of magnetic minerals and, consequently, of iron-rich bioaccumulated particles. Transplants of the lichen *Pseudovernia furfuracea* exposed for 4 months in a complex and heavily polluted area, ranged from  $7.1$  to  $17.1 \times 10^{-8} \text{ m}^3\text{kg}^{-1}$  [37]. Transplants of the same lichen species exposed for 2 months in an industrial area showed values in the range  $0.4$  to  $7.4 \times 10^{-8} \text{ m}^3\text{kg}^{-1}$  [46]. Transplants of *Evernia prunastri* exposed for 6 months around a cement production plant in Slovakia showed magnetic susceptibility ranging  $1.3$  to  $8.1 \times 10^{-8} \text{ m}^3\text{kg}^{-1}$  [47]. Bags of *Parmotrema pilosum* exposed to atmospheric pollutants over the course of 1 year increased from an initial mass-specific magnetic susceptibility value (mean  $\pm$  S.D.) of  $24.1 \pm 5.0 \times 10^{-8} \text{ m}^3\text{kg}^{-1}$  to higher values up to  $51.2 \pm 23.0 \times 10^{-8} \text{ m}^3\text{kg}^{-1}$  [48]. This dataset included three sites, two at metallurgical factories, and one influenced by vehicular emissions, where values increased by 100%.

As emerged from the hysteresis loops, which are very similar and differ only for the concentration-dependent magnetic parameters, which follow the same trend of magnetic susceptibility, the variations of magnetic susceptibility are linked to different concentrations of magnetic particles similar for composition and grain size. The coercivities range, the low saturation field and the SIRM/k values, spanning  $2.4\text{--}7.1 \text{ kA/m}$ , all suggest that magnetite-like minerals are the main magnetic carriers.

In the Day Plot, the lichens transplanted in Milan have been compared to the previous points obtained for *Quercus ilex* leaves sampled in Rome, Italy, PM filters and dusts arising from fuel exhausts and brakes’ emissions, as discussed in [32]. The transplants markedly overlap the “brake” samples

and fall at the lower right end of the cluster defined by the particles accumulated on leaves and filters, in a region of the plot falling in-between the theoretical trends for SD-MD and SD-SP pure magnetites, far from “diesel” and “gasoline” exhausts, which instead follow the theoretical trends for mixtures of single domain (SD) and multidomain (MD) magnetites. This result is at variance with the observations of [37] for combustion dusts accumulated by lichens exposed in an area subjected to arsons, where the magnetic mineralogy corresponded to magnetite-like minerals in PSD magnetic domain state/grain size, similarly to the diesel exhaust emissions in [32].

Also the SIRM/k values ( $5.0 \pm 1.2$  kA/m) are compatible with the brake emissions ( $6.7 \pm 2.5$  kA/m) and distinct from gasoline and diesel emissions ( $13.8 \pm 6.3$  kA/m and  $14.5 \pm 12.1$  kA/m, respectively) reviewed in [49]. Even FORC diagrams confirm the uniform prevalence, irrespective of the concentration, of viscous components of magnetization, closely resembling the diagrams for brakes and leaves reported by [32].

It is recalled that the critical magnetic grain size transitions, theoretically determined for equidimensional magnetite, are about  $0.03 \mu\text{m}$  for SP to SD,  $0.08 \mu\text{m}$  for SD to PSD, and  $17 \mu\text{m}$  for PSD to true MD [50]. Overall, it is not easy to attribute these magnetic features to SP or MD particles. In this sense, none of the magnetic properties diagnostic of the relevant presence of SP particles—e.g., the enhancement of magnetic susceptibility, very low SIRM/k values, asymmetry along the Bu axis in FORC diagrams—supported the presence of ultrafine magnetic particles, although the latter could be linked to the choice of a relatively high averaging time (300 ms) during the measurements. As a further difficulty, in traffic-related PM, the SP fraction may occur as coating of MD particles and is originated by localized stress in the oxidized outer shell surrounding the unoxidized core of magnetite-like grains; thus it cannot be considered as a direct proxy for the overall content of ultrafine  $<30$  nm particles [17].

On the other hand, the presence of clusters of fine and ultrafine magnetic particles is clearly shown by SEM observations; thus, the “intermediate” position in the Day plot might depend both on the chemically-impure composition of the magnetite-like particles and on the coexistence of SP and MD granulometric fractions.

The strength of the statistical associations between magnetic parameters and bioaccumulation of chemical elements corroborated the above conclusions that the main source of air pollution in Milan is non-exhaust emission from vehicular traffic, notably brake abrasions. The deposition of PM enriched in Fe, Cr, Cu, and Sb caused the bioaccumulation of these chemical elements and determined the magnetic susceptibility of lichen samples.

According to their strong intercorrelations,  $k$ ,  $M_s$  and  $M_{rs}$  are indicative of the same magnetic fraction; thus, magnetic susceptibility is a valid, representative and fast proxy for the concentration of ferromagnetic particles associated with trace metals in PM.

Brake wear debris comprises primarily carbonaceous and metal-bearing components, including, besides Fe, heavy metals such as Cu, Sb, Sn, Cd, Cr, Pb, and Zn [43]. In [49], it was shown that Fe-bearing particles result from the friction between a brake pad and the cast iron brake disc; at brake pad temperatures below  $200^\circ\text{C}$ , abrasive processes dominate, and wear particles  $>1 \mu\text{m}$  are mostly generated. At higher operational temperatures ( $>190^\circ\text{C}$ ), the concentration of nanoparticles ( $<100$  nm) increases due to evaporation, condensation and aggregation processes, increasing by four to six orders of magnitude the emission rate of particles, thus constituting  $>90\%$  of total brake dusts and constituting a major source of airborne magnetic nanoparticles. It is possible to speculate that the coexistence of SP and MD particles is the result of both processes, and that SP particles, for their intrinsically deciduous magnetic properties, are more difficult to be seen with standard room temperature magnetic measurements.

As suggested by the relationship between Al and Fe, some proportion of these two metals may also originate from soil resuspension. This is quite common, and in addition, it is known that, although it is well known that brake wear constitutes one of the main sources of non-exhaust roadside PM, brake wear accounts for  $50\%$ – $60\%$  of the total non-exhaust emissions [51].

## 5. Conclusions

From the present results, it is possible to conclude that magnetic properties of lichen transplants are a robust proxy for the bioaccumulation of trace metals. The linear regression model with magnetic susceptibility, as determined by the magnetic fraction of PM, explained large proportions of variance for Fe, Cr, Cu, and Sb accumulated by *E. prunastri*. Chemical, magnetic and morphoscopic analysis clearly pinpointed non-exhaust sources of vehicular traffic, notably brake abrasion, with a broad grain-size range, as the main driver of PM air pollution in Milan.

The above relationships and the strong association of magnetic susceptibility with the concentration-dependent hysteresis parameters suggest that magnetic susceptibility is a simple, fast and very useful parameter that allows time- and cost-effective analysis of air pollution using lichen transplants.

**Author Contributions:** S.L. and A.W. conceived and designed the experiments; T.C., A.V., S.S. and A.W. performed the experiments; S.L. and A.W. analyzed the data; A.B. contributed analysis tools; S.L. and A.W. wrote the paper. All authors have read and agreed to the published version of the manuscript.

**Funding:** Part of this research (magnetic analyses) was funded in the framework of FISIR2016 project, promoted by MIUR, the Italian Ministry of Education, University and Research.

**Conflicts of Interest:** The authors declare no conflict of interest. The funders had no role in the design of the study; in the collection, analyses, or interpretation of data; in the writing of the manuscript, or in the decision to publish the results.

## References

1. WHO (World Health Organization). Available online: [http://www.who.int/gho/phe/outdoor\\_air\\_pollution/en/](http://www.who.int/gho/phe/outdoor_air_pollution/en/) (accessed on 18 March 2020).
2. Forsberg, B.; Hansson, H.C.; Johansson, C.; Areskoug, H.; Persson, K.; Jarvholm, B. Comparative health impact assessment of local and regional particulate air pollutants in Scandinavia. *Ambio* **2005**, *34*, 11–19. [[CrossRef](#)] [[PubMed](#)]
3. Karagulian, F.; Belis, C.A.; Dora, C.F.C.; Prüss-Ustün, A.M.; Bonjour, S.; Adair-Rohani, H.; Amann, M. Contributions to cities' ambient particulate matter (PM): A systematic review of local source contributions at global level. *Atmos. Environ.* **2015**, *120*, 475–483. [[CrossRef](#)]
4. Loppi, S. Lichens as sentinels for air pollution at remote alpine areas (Italy). *Environ. Sci. Pollut. Res.* **2014**, *21*, 2563–2571. [[CrossRef](#)] [[PubMed](#)]
5. Loppi, S.; Paoli, L. Comparison of the trace element content in transplants of the lichen *Evernia prunastri* and in bulk atmospheric deposition: A case study from a low polluted environment (C Italy). *Biologia* **2015**, *70*, 460–466. [[CrossRef](#)]
6. Loppi, S.; Frati, L.; Paoli, L.; Bigagli, V.; Rossetti, C.; Bruscoli, C.; Corsini, A. Biodiversity of epiphytic lichens and heavy metal contents of *Flavoparmelia caperata* thalli as indicators of temporal variations of air pollution in the town of Montecatini Terme (central Italy). *Sci. Total Environ.* **2004**, *326*, 113–122.
7. Loppi, S. May the diversity of epiphytic lichens be used in environmental forensics? *Diversity* **2019**, *11*, 36. [[CrossRef](#)]
8. Contardo, T.; Giordani, P.; Paoli, L.; Vannini, A.; Loppi, S. May lichen biomonitoring of air pollution be used for environmental justice assessment? A case study from an area of N Italy with a municipal solid waste incinerator. *Environ. Forensics* **2018**, *19*, 265–276. [[CrossRef](#)]
9. Loppi, S.; Ravera, S.; Paoli, L. Coping with uncertainty in the assessment of atmospheric pollution with lichen transplants. *Environ. Forensics* **2019**, *20*, 228–233. [[CrossRef](#)]
10. Maher, B.A.; Ahmed, I.A.M.; Karloukovski, V.; MacLaren, D.A.; Foulds, P.G.; Allsop, D.; Mann, D.M.A.; Torres-Jardón, R.; Calderon-Garciduenas, L. Magnetite pollution nanoparticles in the human brain. *Proc. Natl. Acad. Sci. USA* **2016**, *113*, 10797–10801. [[CrossRef](#)]
11. Calderón-Garcidueñas, L.; González-macié, A.; Mukherjee, P.S.; Reynoso-Robles, R.; Pérez-Guillé, B.; Gayosso-Chávez, C.; Torres-Jardón, R.; Cross, J.V.; Ahmed, I.A.M.; Karloukovski, V.V.; et al. Combustion- and friction derived magnetic air pollution nanoparticles in human hearts. *Environ Res.* **2019**, *176*. [[CrossRef](#)]

12. Hofman, J.; Maher, B.A.; Muxworthy, A.R.; Wuyts, K.; Castanheiro, A.; Samson, R. Biomagnetic monitoring of atmospheric pollution: A review of magnetic signatures from biological sensors. *Environ. Sci. Technol.* **2017**, *51*, 6648–6664. [[CrossRef](#)] [[PubMed](#)]
13. Loppi, S.; Pacioni, G.; Olivieri, N.; Di Giacomo, F. Accumulation of trace metals in the lichen *Evernia prunastri* transplanted at biomonitoring sites in central Italy. *Bryologist* **1998**, *101*, 451–454. [[CrossRef](#)]
14. Paoli, L.; Fačkovcová, Z.; Guttová, A.; Maccelli, C.; Kresáňová, K.; Loppi, S. Evernia goes to school: Bioaccumulation of heavy metals and photosynthetic performance in lichen transplants exposed indoors and outdoors in public and private environments. *Plants* **2019**, *8*, 125. [[CrossRef](#)] [[PubMed](#)]
15. Vannini, A.; Paoli, L.; Nicolardi, V.; Di Lella, L.A.; Loppi, S. Seasonal variations in intracellular trace element content and physiological parameters in the lichen *Evernia prunastri* transplanted to an urban environment. *Acta Bot. Croat.* **2017**, *76*, 171–176. [[CrossRef](#)]
16. Sagnotti, L.; Winkler, A. On the magnetic characterization and quantification of the superparamagnetic fraction of traffic-related urban airborne PM in Rome, Italy. *Atmos. Environ.* **2012**, *59*, 131–140. [[CrossRef](#)]
17. Wang, X.; Løvlie, R.; Zhao, X.; Yang, Z.; Jiang, F.; Wang, S. Quantifying ultrafine pedogenic magnetic particles in Chinese loess by monitoring viscous decay of superparamagnetism. *Geochem. Geophys. Geosyst.* **2010**, *11*, 10. [[CrossRef](#)]
18. Day, R.; Fuller, M.; Schmidt, V.A. Hysteresis properties of titanomagnetites: Grain-size and compositional dependence. *Phys. Earth Planet. Inter.* **1977**, *13*, 260–267. [[CrossRef](#)]
19. Dunlop, D.J. Theory and application of the Day plot (MRS/MS versus HCR/HC) 1. Theoretical curves and tests using titanomagnetite data. *J. Geophys. Res.* **2002**, *107*. [[CrossRef](#)]
20. Dunlop, D.J. Theory and application of the Day plot (MRS/MS versus HCR/HC) 2. Application to data for rocks, sediments, and soils. *J. Geophys. Res.* **2002**, *107*. [[CrossRef](#)]
21. Pike, C.R.; Roberts, A.P.; Verosub, K.L. Characterizing interactions in fine magnetic particle systems using first order reversal curves. *J. Appl. Phys.* **1999**, *85*, 6660–6667. [[CrossRef](#)]
22. Roberts, A.; Pike, C.R.; Verosub, K.L. First-order reversal curve diagrams: A new tool for characterizing the magnetic properties of natural samples. *J. Geophys. Res.* **2000**, *105*, 28461–28475. [[CrossRef](#)]
23. Harrison, R.J.; Feinberg, J.M. FORCinel: An improved algorithm for calculating first-order reversal curve distributions using locally weighted regression smoothing. *Geochem. Geophys. Geosyst.* **2008**, *9*. [[CrossRef](#)]
24. Feckler, A.; Low, M.; Zubrod, J.P.; Bundschuh, M. When significance becomes insignificant: Effect sizes and their uncertainties in Bayesian and frequentist frameworks as an alternative approach when analyzing ecotoxicological data. *Environ. Toxicol. Chem.* **2018**, *37*, 1949–1955. [[CrossRef](#)] [[PubMed](#)]
25. Gelman, A.; Goodrich, B.; Gabry, J.; Vehtari, A. R-squared for Bayesian regression models. *Am. Stat.* **2019**, *73*, 307–309. [[CrossRef](#)]
26. Selya, A.S.; Rose, J.S.; Dierker, L.C.; Hedeker, D.; Mermelstein, R.J. A practical guide to calculating Cohen's  $f^2$ , a measure of local effect size, from proc mixed. *Front. Psychol.* **2012**, *3*, 111. [[CrossRef](#)] [[PubMed](#)]
27. Cohen, J.E. *Statistical Power Analysis for the Behavioral Sciences*; Lawrence Erlbaum Associates, Inc.: Hillsdale, NJ, USA, 1988.
28. R Core Team. *R: A Language and Environment for Statistical Computing*; R Foundation for Statistical Computing: Vienna, Austria, 2020; Available online: <https://www.R-project.org/> (accessed on 18 March 2020).
29. Cecconi, E.; Fortuna, L.; Benesperi, R.; Bianchi, E.; Brunialti, G.; Contardo, T.; Di Nuzzo, L.; Frati, L.; Monaci, F.; Munzi, S.; et al. New interpretative scales for lichen bioaccumulation data: The Italian proposal. *Atmosphere* **2019**, *10*, 136. [[CrossRef](#)]
30. Szönyi, M.; Sagnotti, L.; Hirt, A.M. On leaf magnetic homogeneity in particulate matter biomonitoring studies. *Geophys. Res. Lett.* **2007**, *34*, L06306. [[CrossRef](#)]
31. Sagnotti, L.; Macrì, P.; Egli, R.; Mondino, M. Magnetic properties of atmospheric particulate matter from automatic air sampler stations in Latium (Italy): Toward a definition of magnetic fingerprints for natural and anthropogenic PM10 sources. *J. Geophys. Res.* **2006**, *111*, B12. [[CrossRef](#)]
32. Sagnotti, L.; Taddeucci, J.; Winkler, A.; Cavallo, A. Compositional, morphological, and hysteresis characterization of magnetic airborne particulate matter in Rome, Italy. *Geochem. Geophys. Geosyst.* **2009**, *10*. [[CrossRef](#)]
33. Sarbak, Z.; Stanczyk, A.; Kramer-Wachowiak, M. Characterization of surface properties of various fly ashes. *Powder Technol.* **2004**, *145*, 82–87. [[CrossRef](#)]

34. Veneva, L.; Hoffmann, V.; Jordanova, D.; Jordanova, N.; Fehr, T. Rock magnetic, mineralogical and micro-structural characterization of fly ashes from Bulgarian power plants and the nearby anthropogenic soils. *Phys. Chem. Earth* **2004**, *29*, 1011–1023. [[CrossRef](#)]
35. Jordanova, D.; Hoffmann, V.; Fehr, K.T. Mineral magnetic characterization of anthropogenic magnetic phases in the Danube river sediments (Bulgarian parts). *Earth Planet. Sci. Lett.* **2004**, *221*, 71–89. [[CrossRef](#)]
36. Jordanova, D.; Jordanova, N.; Hoffmann, V. Magnetic mineralogy and grain-size dependence of hysteresis parameters of single spherules from industrial waste products. *Phys. Earth Planet. Inter.* **2006**, *154*, 255–265. [[CrossRef](#)]
37. Winkler, A.; Caricchi, C.; Guidotti, M.; Owczarek, M.; Macrì, P.; Nazzari, M.; Amoroso, A.; Di Giosa, A.; Listrani, S. Combined magnetic, chemical and morphoscopic analyses on lichens from a complex anthropic context in Rome, Italy. *Sci. Total Environ.* **2019**, *690*, 1355–1368. [[CrossRef](#)]
38. Loppi, S.; Pirintsos, S.A.; De Dominicis, V. Soil contribution to the elemental composition of epiphytic lichens (Tuscany, central Italy). *Environ. Monit. Assess.* **1999**, *58*, 121–131. [[CrossRef](#)]
39. Giordano, S.; Adamo, P.; Sorbo, S.; Vingiani, S. Atmospheric trace metal pollution in the Naples urban area based on results from moss and lichen bags. *Environ. Pollut.* **2005**, *136*, 431–442. [[CrossRef](#)]
40. Loppi, S.; Corsini, A.; Paoli, L. Estimating environmental contamination and element deposition at an urban area of central Italy. *Urban Sci.* **2019**, *3*, 76. [[CrossRef](#)]
41. Paoli, L.; Munzi, S.; Fiorini, E.; Gaggi, C.; Loppi, S. Influence of angular exposure and proximity to vehicular traffic on the diversity of epiphytic lichens and the bioaccumulation of traffic-related elements. *Environ. Sci. Pollut. Res.* **2013**, *20*, 250–259. [[CrossRef](#)]
42. Vannini, A.; Paoli, L.; Russo, A.; Loppi, S. Contribution of submicronic (PM<sub>1</sub>) and coarse (PM > 1) particulate matter deposition to the heavy metal load of lichens transplanted along a busy road. *Chemosphere* **2019**, *231*, 121–125. [[CrossRef](#)]
43. Bonfanti, A. Low-Impact Friction Materials for Brake Pads. Ph.D. Thesis, University of Trento, Trento, Italy, June 2016.
44. Thorpe, A.; Harrison, R. Sources and properties of non-exhaust particulate matter from road traffic: A review. *Sci. Total Environ.* **2008**, *400*, 270–282. [[CrossRef](#)]
45. Sanders, P.G.; Xu, N.; Dalka, T.M.; Maricq, M.M. Airborne brake wear debris: Size distributions, composition, and a comparison of dynamometer and vehicle tests. *Environ. Sci. Technol.* **2003**, *37*, 4060–4069. [[CrossRef](#)] [[PubMed](#)]
46. Kodnik, D.; Candotto Carniel, F.; Licen, S.; Tolloi, A.; Barbieri, P.; Tretiach, M. Seasonal variations of PAHs content and distribution patterns in a mixed land use area: A case study in NE Italy with the transplanted lichen *Pseudevernia furfuracea*. *Atmos. Environ.* **2015**, *113*, 255–263. [[CrossRef](#)]
47. Paoli, L.; Winkler, A.; Guttová, A.; Sagnotti, A.; Grassi, A.; Lackovičová, A.; Senko, D.; Loppi, S. Magnetic properties and element concentrations in lichens exposed to airborne pollutants released during cement production. *Environ. Sci. Pollut. Res.* **2017**, *24*, 12063–12080. [[CrossRef](#)] [[PubMed](#)]
48. Marié, D.C.; Chaparro, M.A.E.; Sinito, A.M. Magnetic biomonitoring of airborne particles using lichen transplants over controlled exposure periods. *SN Appl. Sci.* **2020**, *2*, 104. [[CrossRef](#)]
49. Gonet, T.; Maher, B.A. Airborne, vehicle-derived Fe-bearing nanoparticles in the urban environment—A review. *Environ. Sci. Technol.* **2019**, *53*, 9970–9991. [[CrossRef](#)]
50. Butler, R.F.; Banerjee, S.K. Theoretical single-domain grain size range in magnetite and titanomagnetite. *J. Geophys. Res.* **1975**, *80*, 4049–4058. [[CrossRef](#)]
51. Harrison, R.M.; Jones, A.M.; Gietl, J.; Yin, J.; Green, D.C. Estimation of the contributions of brake dust, tire wear, and resuspension to nonexhaust traffic particles derived from atmospheric measurements. *Environ. Sci. Technol.* **2012**, *46*, 6523–6529. [[CrossRef](#)]

